View metadata, citation and similar papers at core.ac.uk

brought to you by CORE

provided by Crossref

Shock and Vibration 17 (2010) 759–770
DOI 10.3233/SAV-2010-0519
IOS Press

Dynamics of nonlinear coupled electrostatic micromechanical resonators under two-frequency parametric and external excitations

Wen-Ming Zhang*, Guang Meng and Ke-Xiang Wei
State Key Laboratory of Mechanical System and Vibration, School of Mechanical Engineering, Shanghai Jiao Tong University, 800 Dongchuan Road, Shanghai 200240, P.R. China

Received 8 May 2009
Revised 31 August 2009

Abstract. In this paper, nonlinear dynamics and chaos of electrostatically actuated MEMS resonators under two-frequency parametric and external excitations are investigated analytically and numerically. A nonlinear mass-spring-damping model is used to accounting for squeeze film damping and the parallel plate electrostatic force. The micro-structure is excited by a dc bias electrostatic force and a harmonic force with a frequency tuned closely to their fundamental natural frequencies (combination oscillation). The quality factor is calculated for the microcantilever beam of the resonator considering squeeze film damping. The effect of nonlinear squeeze film damping on the frequency response, quality factor, resonant frequency and nonlinear dynamic characteristics of the dynamic system are provided with numerical simulations using the bifurcation diagram, Poicare maps, largest Lyapunov exponent and phase portrait. The results show that the dynamic system goes through a complex nonlinear vibration as the system parameters change. It is indicated that the effect of nonlinear squeeze film damping should be considered due to its decreasing the quality factor and changing the nonlinear phenomena of the MEMS resonators.

Keywords: MEMS, resonator, electrostatic actuation, squeeze film damping, combination oscillation

1. Introduction

Recent technological advances have enabled the fabrication of resonators down to micro- and even nano- scales. The relevance of nanotechnology is well recognized, so new developments and applications based on nonlinear dynamics, chaos, fractals, and nonlinear control, are nowadays reached in an interdisciplinary framework [1,2]. Resonant MEMS devices are widely used to measure strain, force or displacement [3–5]. Electrostatically actuated resonators have the advantages of simple structures that allow easy batch fabrications and they form a major component in many MEMS devices, such as capacitive switch [3], filter [4], and mass sensor [5].

During the past decade, many researchers had paid attention to the applications of parametric excitation for MEMS/NEMS devices [6–26]. Carr et al. [6] and Zalalutdinov et al. [7] studied the parametric amplification of the motion of resonators through electrostatic and optical actuation. However, the reported methods should be used to discuss the instability and control strategies. It is necessary to benefit from the parametric amplification phenomena which had not remarked. A demonstration of the phenomena of parametrically excited vibrations in MEMS/NEMS

*Corresponding author. Tel.: +86 21 3420 6813-818; E-mail: wenmingz@sjtu.edu.cn.

ISSN 1070-9622/10/$27.50 © 2010 – IOS Press and the authors. All rights reserved

was reported in [8,17]. Abdel-Rahman and Nayfeh [9] and Gallacher et al. [10] applied the super-harmonic and combination parametric resonances as suitable excitation methods to minimize electrical “feedthrough”. The phenomenon of the parametric excitation in spatially extended MEMS/NEMS was investigated theoretically by Lifshitz and Cross [11]. Gallacher et al. [12] studied the application of combined external forcing and parametric excitation to the micro-ring gyroscope in order to enable parametric amplification of the dynamic gain of the primary mode by at least two orders of magnitude. Napoli [13] gave the dynamic responses of a parametrically excited micro-cantilever using the linear and nonlinear Mathieu equations. The study on the array of parametrically excited strings were carried out both experimentally [14] and theoretically [11]. Hu et al. [15] discussed the resonances of electrostatically actuated micro-cantilevers, while Baskaran and Turner [16] demonstrated the coupled modes parametric resonance. It should be noted, however, that an important feature of parametric excitation is the ability of stabilizing a statically unstable system. Krylov et al. [18] investigated the possibility of parametric stabilization of electrostatically actuated microstructures under the effects of ac component and dc component voltages. Younis and Nayfeh [19] and Abdel-Rahman and Nayfeh [9] studied the dynamic responses of an electrostatically resonator to a primary-resonance excitation [19], a superharmonic-resonance excitation of order two [9], and a subharmonic-resonance excitation of order one-half [9]. It can be concluded that these models gave accurate results for small ac amplitudes and hence small motions. Younis et al. [3] applied the shooting method to simulate the dynamics of a novel MEMS switch excited near primary resonance and undergoing large motion. Mestrom et al. [23] modelled the dynamics of a MEMS resonator numerically and experimentally considering the effect of thermal noise. Kacem et al. [24] studied the nonlinear dynamics of nanomechanical beam resonators to improve the performance of NEMS-based sensors. Alsaleem et al. [25] investigated the nonlinear phenomena, including primary resonance, superharmonic and subharmonic resonances, in electrostatically actuated resonators both experimentally and theoretically. However, the dynamic response of the electrostatic MEMS resonator to a combination resonance excitation has not been paid more attention in literature. This work aims at extending our previous studies [20,22, 26] and is a step toward modeling and understanding of the nonlinear dynamics of the electrostatically actuated resonator under combination resonant condition with the effect of nonlinear squeeze film damping.

The outline for this paper is as follows. In Section 2, the simplified mass-spring-damping dynamic model of an electrostatically actuated MEMS resonator is presented. In Section 3, perturbation analyses of the governing equation using multiple scale method is given. Additionally, numerical simulations and results of the resonant frequencies, frequency responses, quality factors and nonlinear dynamic properties are described and discussed in Section 4. Finally, some conclusions are drawn in Section 5.

2. Dynamic model

De and Aluru [27,28] suggested that it is easier to understand the physics behind the dynamic properties of electrostatic MEMS with a simpler mass-spring-damping model. Therefore, a microcantilever beam was considered in this work and the electrostatically actuated MEMS structure was $4.5\ um \times 80\ um \times 200\ um$ in dimensions [29], and the dynamic model was shown in Fig. 1. The simplified mass-spring-damping system can be written as

$$m\ddot{x}(t) + c\dot{x}(t) + kx(t) + k_c x(t)^3 = F_e(x,t) + F_s(x,\dot{x}) \tag{1}$$

where m is the mass, k and c are the effective spring stiffness and damping coefficient of the simplified system, respectively, k_c is the cubic nonlinear stiffness, and F_s and F_e are the squeeze film damping force and nonlinear electrostatic force, respectively. The electrostatic force F_e is given by

$$F_e(x,t) = \frac{\varepsilon_0 A_0}{2}\left(\frac{1}{d_0^2} + \frac{2}{d_0^3}x\right)V^2(t) \tag{2}$$

where the input voltage $V(t) = V_{dc} + V_{ac}\cos\omega t$, in which V_{dc} and V_{ac} are dc bias voltage and alternating current (ac) voltage, respectively, ε_0 is the absolute dielectric constant of vacuum ($\varepsilon_0 = 8.85 \times 10^{-12} F/m$), $A_0$is the overlapping area between the two plates, and d_0 is the gap.

The surrounding gas medium plays an important role on the dynamics of the cantilever in MEMS resonators. For a rectangular cantilever beam [30], when the quality factor of the fundamental mode of the cantilever in gas exceeds

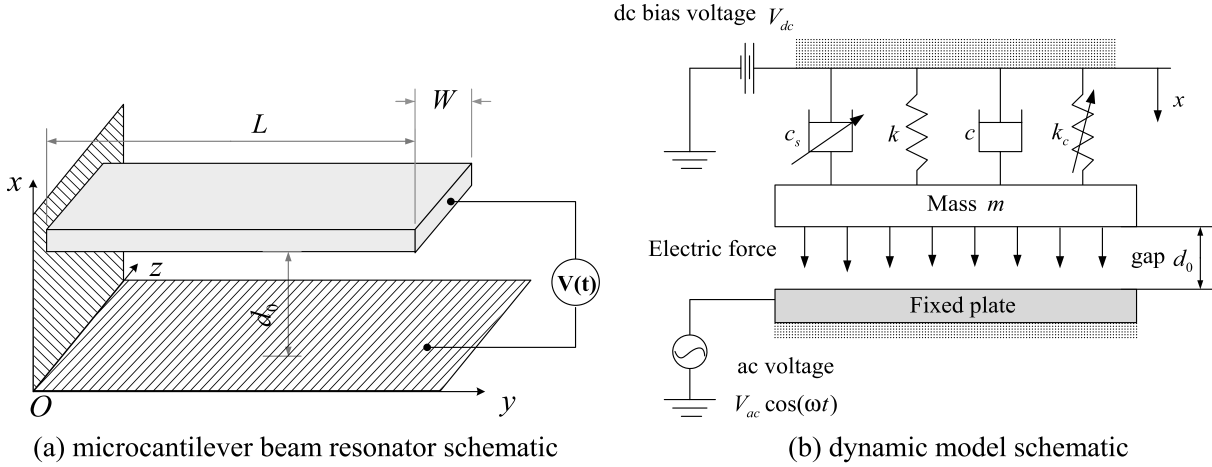

Fig. 1. Simplified dynamic model of a micromechanical electrostatic resonator.

1, which is typically satisfied when the cantilever is placed in air, the relationship between the vacuum resonant frequency ω_{vac} and the resonant frequency in gasω_{gas} can be given by [31]

$$\frac{\omega_{gas}}{\omega_{vac}} = \left(1 + \frac{\pi\rho B}{4\rho_c H}\Gamma_r(\omega_{gas})\right)^{-1/2} = \left(1 + \frac{\pi}{4}\Pi\Gamma_r(\omega_{gas})\right)^{-1/2} \tag{3}$$

where ρ is the density of the gas, the nominal width B is the dominant length scale in the gas flow, ρ_c and H are the density and thickness of the cantilever, respectively, and the natural scaling parameter is $\Pi = \frac{\rho B}{\rho_c H}$. The hydrodynamic functions $\Gamma(\omega)$ is defined as $\Gamma = \Gamma_r + j\Gamma_i$ [30,31], in which $\Gamma_r = a_1 + \frac{a_2}{\sqrt{R_e}}$ and $\Gamma_i = \frac{b_1}{\sqrt{R_e}} + \frac{b_2}{R_e}$, and $a_1 = 1.0553$, $a_2 = 3.7997$, $b_1 = 3.8018$, and $b_2 = 2.7364$ [31].

The quality factor for the bending modes can be written as [31]

$$Q_{gas} = \frac{\frac{4\mu}{\pi\rho B^2} + \Gamma_r(\omega_{gas})}{\Gamma_i(\omega_{gas})} = \frac{\frac{4}{\pi}\cdot\frac{1}{\Pi} + \Gamma_r(\omega_{gas})}{\Gamma_i(\omega_{gas})} \tag{4}$$

At a few microns in size, squeeze film damping should be used to represent the gas-film damping experienced by the moving plates [32,33]. For a rectangular plate, the squeeze film damping force $F_s(x,\dot{x})$ can be given by Taylor series, i.e.

$$F_s(x,\dot{x}) = -c_s\left(\frac{1}{d_0^3} + \frac{3}{d_0^4}x\right)\dot{x} \tag{5}$$

where the effective damping coefficient $c_s = 16\mu C_r W^3 L$, in which μ is the viscous coefficient, and W and L are the width and length of the cantilever, respectively, and $C_r = 1 - 0.6\frac{W}{L}$, $\left(0 < \frac{W}{L} < 1\right)$.

The dimensionless variables are defined as

$$\tau = \omega_n t, \quad \omega_n = \sqrt{k/m}, \quad \Omega = \omega/\omega_n, \quad \zeta = \frac{c}{m\omega_n}, \quad \beta = \frac{c_s\omega_n}{d_0^2}, \quad \gamma = \frac{k_c}{k}d_0^2, \quad X = x/d_0, \quad \dot{X} = dX/d\tau,$$

$$\ddot{X} = d^2X/d\tau^2, \quad a_1 = \frac{\varepsilon_0 A_0}{2m\omega_n^2 d_0^3}\left(V_{dc}^2 + \frac{V_{ac}^2}{2}\right), \quad a_2 = \frac{\varepsilon_0 A_0}{m\omega_n^2 d_0^3}V_{dc}V_{ac}, \quad a_3 = \frac{\varepsilon_0 A_0}{4m\omega_n^2 d_0^3}V_{ac}^2$$

Then, the equation of motion can be rewritten in the dimensionless form as

$$\ddot{X} + \zeta\dot{X} + F_s\left(X,\dot{X}\right) + \left(1 - 2a_1 - 2a_2\cos\Omega\tau - 2a_3\cos 2\Omega\tau\right)X + \gamma X^3 = \sum_{m=1}^{3} a_m\cos\left[(m-1)\Omega\tau\right] \tag{6}$$

3. Perturbation analysis

Let us consider the weakly nonlinear dynamic system and assume $\zeta = \varepsilon\tilde{\zeta}$, $\beta = \varepsilon\tilde{\beta}$, $\gamma = \varepsilon\tilde{\gamma}$ and $a_m = \varepsilon\tilde{a}_m$ ($m = 1 \sim 3$), in which ε is a small parameter. The equation of the motion has the form

$$\ddot{X} + X = \varepsilon\left\{\tilde{F}_s\left(X,\dot{X}\right) - \tilde{\gamma}X^3 - \tilde{\zeta}\dot{X} + 2\sum_{m=1}^{3}\tilde{a}_m\cos\left[(m-1)\Omega\tau\right]\cdot X + \sum_{m=1}^{3}\tilde{a}_m\cos\left[(m-1)\Omega\tau\right]\right\} \quad (7)$$

The desired function $X(\tau)$ can be represented in terms of a series using multiple scale method [34]

$$X(\tau;\varepsilon) = X_0(T_0,T_1) + \varepsilon X_1(T_0,T_1) + \cdots \quad (8)$$

where $T_n = \varepsilon^n\tau$.

Then the first and second derivatives are defined respectively, as follows

$$\frac{d}{d\tau} = D_0 + \varepsilon D_1 + \cdots, \quad \frac{d^2}{d\tau^2} = D_0^2 + 2\varepsilon D_0 D_1 + \cdots \quad (9)$$

where $D_n = {}^{\partial}\!/_{(\partial T_n)}$. Substituting Eqs (9) and (8) into (7), equating the coefficient at equal powers of ε, and limiting ourselves by terms of ε^2, a set of recurrent equations yield

$$D_0^2X_0 + X_0 = \sum_{m=1}^{3}a_m\cos\left[(m-1)\Omega T_0\right] \quad (10)$$

$$D_0^2X_1 + X_1 = -2D_0D_1X_0 - \tilde{\zeta}D_0X_0 + \tilde{F}_{s0} - \tilde{\gamma}X_0^3 + 2\sum_{m=1}^{3}a_m\cos\left[(m-1)\Omega T_0\right]\cdot X_0 \quad (11)$$

where $\tilde{F}_{s0}$ is the damping term and $\tilde{F}_{s0} = -\tilde{\beta}\left(D_0X_0 + 3X_0D_0X_0\right)$.

The general solution of Eq. (10) has the form

$$X_0 = A\cos\left(T_0 + \phi\right) + \sum_{k=0}^{2}\Lambda_k\cos(\omega_k T_0) \quad (12)$$

where $A = A(T_1)$ and $\phi = \phi(T_1)$ are vibration amplitude and phase, respectively, and $\Lambda_k = \frac{a_{k+1}}{1-\omega_k^2}$ and $\omega_k = k\Omega \quad (k = 0, 1, 2)$.

Substituting Eq. (12) into Eq. (11) and eliminating the secular terms from X_1, for the combination resonant condition, $\omega_1 + \omega_2 \approx 1 + \varepsilon\sigma$, i.e. $\omega_2 = 2\omega_1 \approx \frac{2}{3}$, yields

$$\begin{cases} A' = -\frac{1}{2}\Gamma_0 A + \frac{1}{2}\Gamma_1\sin\psi \\ A\phi' = -\frac{1}{2}\left[2Aa_1 - \tilde{\gamma}A\left(\frac{3}{4}A^2 + \Gamma_2\right)\right] - \frac{1}{2}\Gamma_1\cos\psi \end{cases} \quad (13)$$

where $\Gamma_0 = \tilde{\zeta} + \tilde{\beta} + 3\tilde{\beta}\Lambda_0$, $\Gamma_1 = a_2\Lambda_2 + a_3\Lambda_1 - 3\tilde{\gamma}\Lambda_0\Lambda_1\Lambda_2$, $\Gamma_2 = 3\Lambda_0^2 + \frac{3}{2}\Lambda_1^2 + \frac{3}{2}\Lambda_2^2$ and $\psi = \sigma T_1 - \phi$.

For the steady-state motion at $a' = \psi' = 0$, that is the singular points of Eq. (13), the frequency response of the system under combination oscillations can be obtained as follows

$$\left[4\Gamma_0^2 + \left(4\sigma + 2a_1 - 2\tilde{\gamma}\Gamma_2 - \frac{3}{2}\tilde{\gamma}A^2\right)^2\right]A^2 = 4\Gamma_1^2 \quad (14)$$

Equation (14) is an implicit equation for the amplitude of the response A as a function of the detuning parameter σ and other parameters, including γ, β, V_{dc}, V_{ac} and d_0.

4. Numerical simulation results and discussion

In this section, numerical simulations on the important dynamic characteristics of the electrostatically actuated MEMS resonator, including resonant frequency, frequency response and nonlinear dynamics, are given in detail. The selected parameters are as follows: $m = 3.5 \times 10^{-11}kg$, $k = 0.17N/m$, $c = 1.78 \times 10^{-6}kg/s$ and $A_0 = 1.6 \times 10^{-9}m^2$ [29].

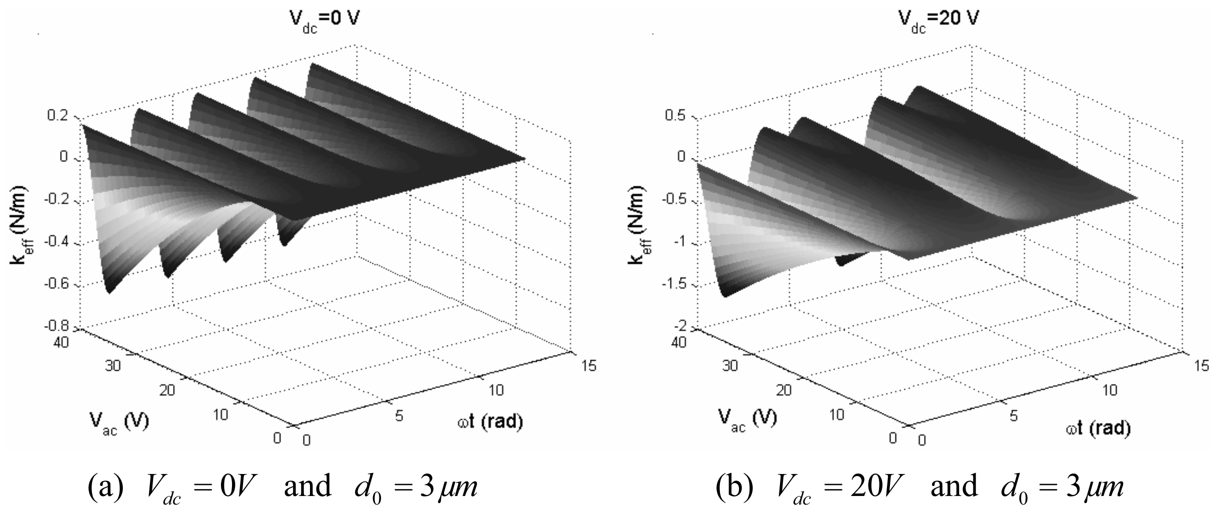

Fig. 2. Relationships between the effective stiffness and the dc bias voltage and the ac voltage: (a) $V_{dc} = 0V$ and $d_0 = 3\ \mu m$; (b) $V_{dc} = 20V$ and $d_0 = 3\ \mu m$.

4.1. Resonant frequency

Resonant frequency is one of the important parameter confirming the exerted force in MEMS devices. It depends on both the electrostatic force and the deformation of the MEMS resonant structure. The nonlinearity in spring stiffness includes a combination of softening material nonlinearities and hardening geometric nonlinearities. The relative "spring-softening" or "spring-hardening" effect of the electrostatic force can be explained by the analytical expression (2). $F_e(t)$ is only a function of $V(t)$ at small displacements. However, with the increase of $V(t)$, x/d_0 increases and, hence, $F_e(t)$ depends on x as well. As a result, the electrostatic force $F_e(t)$ acts like a negative spring, which leads to "spring-softening".

It can be obtained from Eqs (1) and (2) that the effective stiffness $k_{eff} = k - \frac{\varepsilon_0 A_0}{d_0^3}\left(V_{dc} + V_{ac}\cos\omega t\right)^2$. The expression indicates that k_{eff} is a periodically time-varying function depending on the dc bias and ac voltages and gap. The electrostatic force softens the stiffness of the MEMS resonant structure periodically. Numerical simulations of the effective stiffness k_{eff} can be seen from Fig. 2. Figure 2(a) illustrates that the effective stiffness decrease periodically with the increase of the frequency ω of the ac voltage and the variation increases with larger magnitude of the ac voltage V_{ac} when $V_{dc} = 0V$ and $d_0 = 3\ \mu m$. When the dc bias voltage V_{dc} is considered, $V_{dc} = 20V$, the effective stiffness also decrease periodically but with two-frequency components (ω and 2ω) as shown in Fig. 2(b). It is demonstrated that the effective stiffness decreases periodically with the increase of the ac voltage and dc bias voltage.

Figure 3 gives the relationship between the first resonant frequency and dc bias voltage when the ac voltage $V_{ac} = 0V$ at different gaps for the MEMS resonator. It can be observed the "spring-softening" at three different gaps and indicated that the mechanical nonlinearity is absent due to the large deformation [28]. It is also shown that the resonant frequency increases with the increase of the gap at the same dc bias voltage. In addition, the resonant frequency is a monotonically decreasing function of increasing dc bias voltage when the ac voltage has not been considered in this case.

4.2. Quality factor

Squeeze film damping is one of the key parameters for the dynamic responses of the micro-devices. The larger the squeeze film damping is, the higher the noise level is led to. It can be obtained from Eq. (3) that the numerically simulations of the ratio of the fundamental resonant frequency in gas to that in vacuum $\omega_{gas}/\omega_{vac}$.

Figure 4 shows the ratio of resonant frequencies in vacuum and gas $\omega_{gas}/\omega_{vac}$ as a function of the Reynolds number R_e at different natural scaling parameter Π. It can be seen from Fig. 4 that $\omega_{gas}/\omega_{vac}$ is increasing with

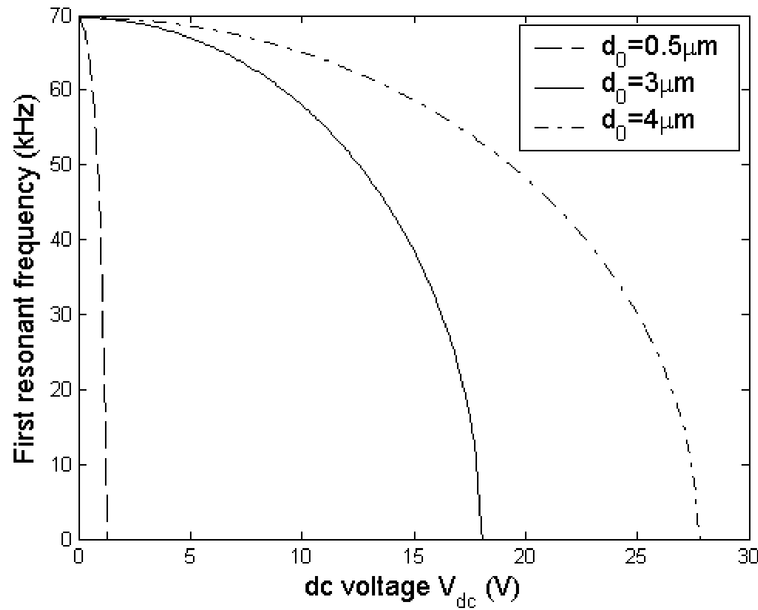

Fig. 3. Relationship between the first resonant frequency with the ac voltage at $V_{ac} = 0V$ and different gaps.

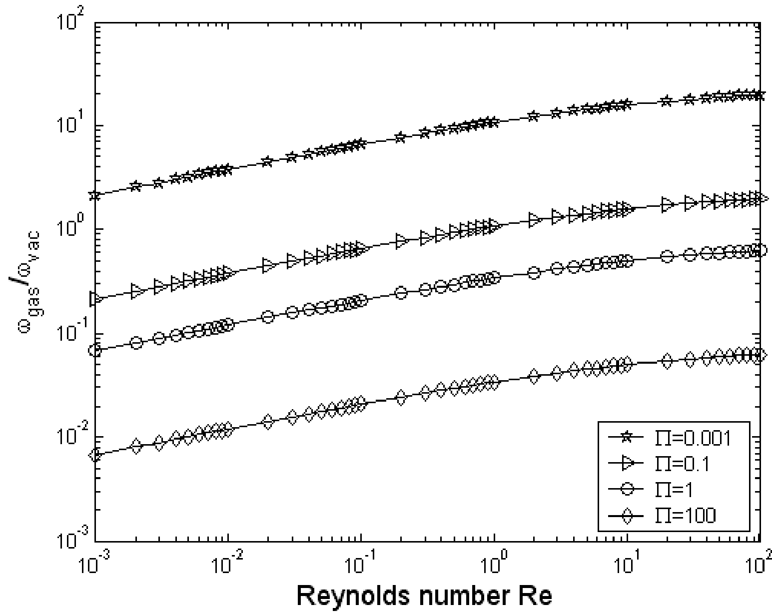

Fig. 4. Relationship between the vacuum resonant frequency ω_{vac} and the resonant frequency in gas ω_{gas} ($\omega_{gas}/\omega_{vac}$) as a function of the Reynolds number R_e at different natural scaling parameter Π.

the increase of Reynolds number R_e and $\omega_{gas}/\omega_{vac}$ decreases with the increase of the scaling parameter Π. We can obtain from Eq. (4) that the quality factor Q_{gas} as a function of both natural scaling parameters, R_e and Π, as illustrated in Fig. 5. It is indicated that the quality factor Q_{gas} increases with the increase of the Reynolds number R_e and the decrease of the natural scaling parameter Π. Meanwhile, when the natural scaling parameter Π tends to be a larger value (in the case of $\Pi = 10$), the quality factor Q_{gas} has small change. As displayed in Fig. 5, when Π changes from 10 to 100, the quality factor Q_{gas} has very small change.

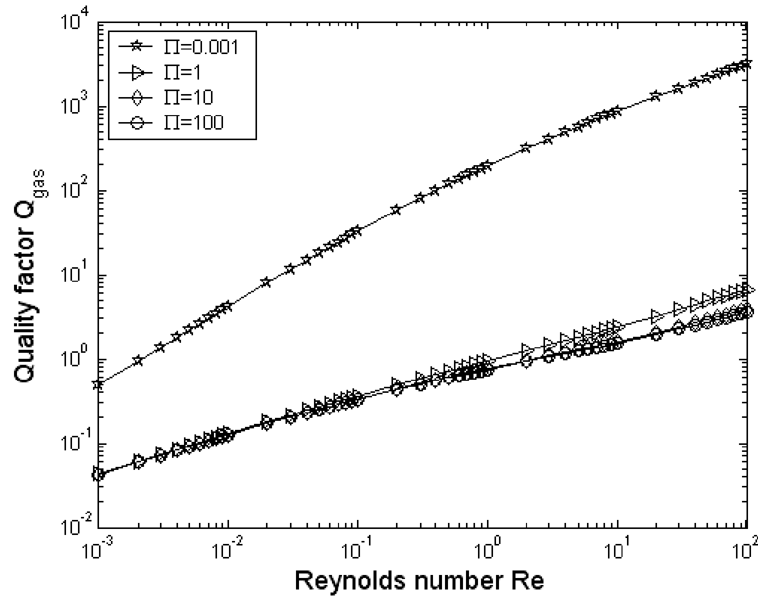

Fig. 5. Quality factor Q_{gas} as a function of the Reynolds number R_e for the fundamental mode at different natural scaling parameter Π.

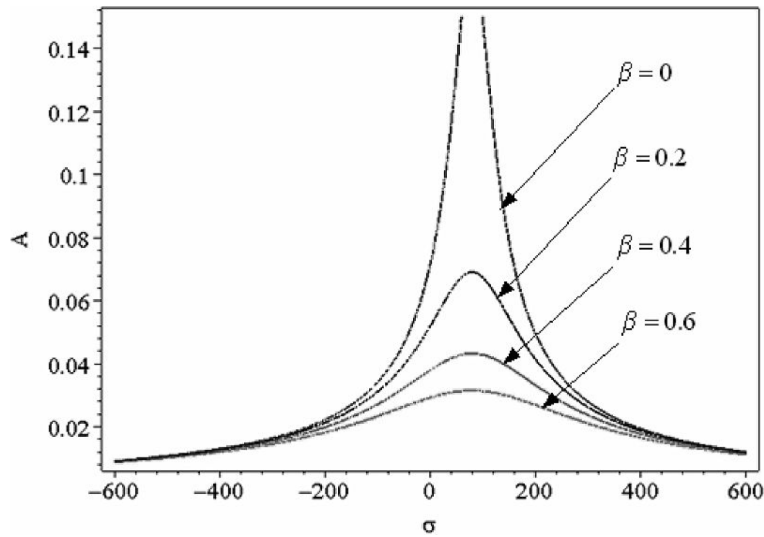

Fig. 6. Effect of squeeze film damping on frequency response at $\gamma = 0.2$, $V_{dc} = 30V$, $V_{ac} = 10V$ and $\varepsilon = 0.01$.

4.3. *Frequency responses*

It can be seen from Eq. (14) that the frequency response of a MEMS resonant structure is governed by the dc bias voltage, the ac voltage, as well as the squeeze film damping and the gap. To demonstrate the dependency of the steady-state behavior of the MEMS device, the frequency response for nonlinear squeeze film damping are illustrated graphically.

Figure 6 shows the variation of the squeeze film damping on the frequency response of the MEMS resonator. It should be noted that, in the absence of damping, the peak amplitude is infinite and the frequency response curve consists of two branches having as their asymptotes. With the increasing the damping, the amplitude of the oscillation can diminish as expected as possible. Therefore, decreasing the damping will result in the increase of the quality

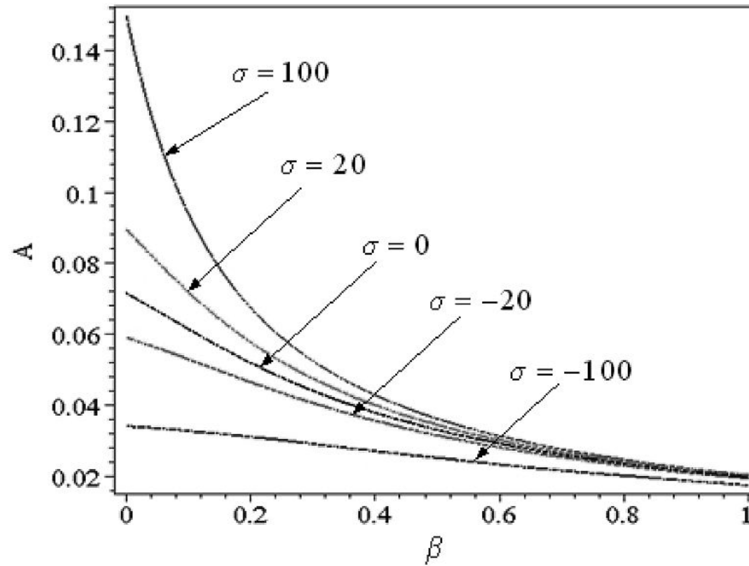

Fig. 7. Amplitude of the response as a function of the squeeze film damping for several values of σ.

factor of the resonant structure, which is considered a positive phenomenon. The effect of damping has two main roles in MEMS dynamics. It could be used to control the system remaining within the physical boundary $X < 1$, and it must be as low as possible to increase the quality factor of the resonator.

Figure 7 illustrates the variation of the amplitude of the response with the squeeze film damping at several values of σ, in which the values of $\gamma = 0.2$, $V_{dc} = 30V$ and $V_{ac} = 10V$ are the same for all curves. It can be found that these curves can be obtained directly from Eq. (14). It should be note that all the curves are single-valued depending on the value of σ. It shows from the frequency response that dc bias and ac voltages have softening effects and shift the resonant frequency to the lower values. In addition, the squeeze film damping has the least effect on resonant frequency with high effects on decreasing the peak amplitudes of the response of the resonator.

4.4. Bifurcation and chaos behavior

This section aims at numerically investigating nonlinear dynamics of a electrostatically actuated MEMS resonator. The 4th order Runge-Kutta method is used to integrate the set of Eq. (6). A small integration step (2π/200) has to be chosen to ensure a stable solution and to avoid the numerical divergence at the points where derivatives of F_e and F_s are discontinuous. The effects of system parameters on the dynamic behavior of the cantilever vibrating system are investigated by using the bifurcation diagram, Poincaré maps, largest Lyapunov exponent, phase portraits, time histories and amplitude spectrum.

Squeeze film damping coefficient and ratio are the key parameters for the dynamic responses of the MEMS devices. The larger the squeeze film damping, the louder noise will exist. Considering the effect of squeeze film damping coupling with the electrostatic force on the system response and using the squeeze film damping as the control parameter which ranges from 0.0 to 1.0, Figs 8 and 9 display the bifurcation diagrams and largest Laypunov exponent maps of squeeze film damping ratio β for the coupling nonlinear dynamic system with different applied voltages, i.e. $V_{dc} = 0$ and $V_{ac} = 40$V, and $V_{dc} = 40$V and $V_{ac} = 40$V.

It can be seen from Figs 8 and 9 that the system response changes between periodic and chaotic motion alternatively when $\beta < 0.2$, and then it enters into synchronous with period-1 when $\beta > 0.2$. In addition, with the increase of dc bias voltage V_{dc}, we can find that the chaotic motion components increases and shifts to the lower squeeze film damping ratio. It is indicated that reasonable increase of dc bias voltage can reduce the effect of nonlinear squeeze film damping on the dynamic response of the coupling system.

Figures 10 and 11 show the Poincare maps and phase plane portraits of different squeeze film damping ratio β on the responses of the coupling system with $V_{dc} = 40$V and $V_{ac} = 40$V. The system response comes into synchronous

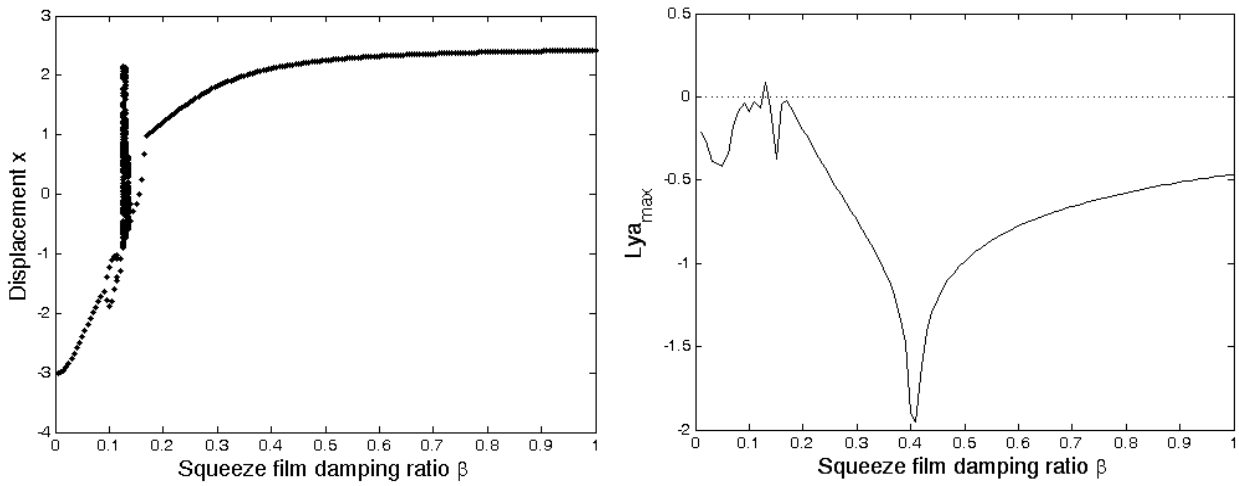

Fig. 8. Bifurcation diagram and largest Laypunov exponent map of β for the coupling nonlinear dynamic system with $V_{dc} = 0$ and $V_{ac} = 40$V.

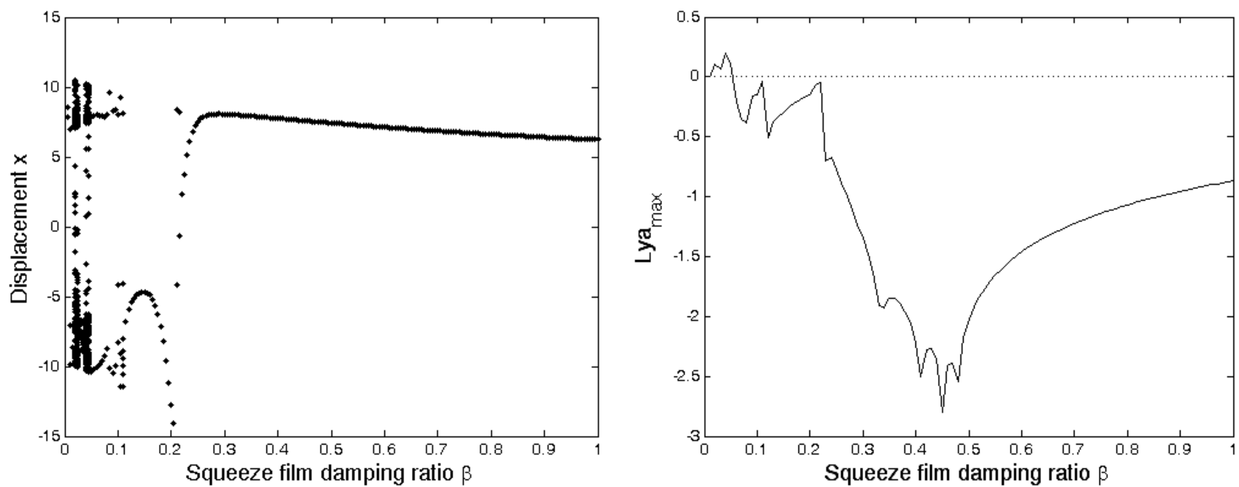

Fig. 9. Bifurcation diagram and largest Laypunov exponent map of β for the coupling nonlinear dynamic system with $V_{dc} = 40$V and $V_{ac} = 40$V.

motion with period-3 at $\beta = 0.1$, as illustrated in Fig. 10(b), from chaotic motion at $\beta = 0.04$, as displayed in Fig. 10(a), then it leaves synchronous motion with period-3 and enters synchronous motion with period-1 when $\beta > 0.2$. At $\beta = 0.04$, the chaos are shown in Fig. 10(a) and Fig. 11(a), the strange attractor has a fractal structure, the corresponding largest Lyapunov exponent is positive. With the increase of squeeze film damping ratio, we can find the period-3 motion with three isolated points in Poincare map and three circles in phase portrait at $\beta = 0.1$, as illustrated in Fig. 10(b) and Fig. 11(b), the corresponding largest Lyapunov exponent becomes negative, which can be seen in Fig. 11. Therefore, the effect of squeeze film damping on the system response can not be neglected for MEMS structures at micro-scale.

The nonlinear dynamic characteristics of the electrostatically actuated MEMS resonators will alter with the change of the ac voltage and dc bias voltage, as shown in Fig. 12. It is indicated that the nonlinear dynamic system displays very rich nonlinear phenomena when the ac voltage and dc bias voltage have been investigated as the control parameters. With the increase of ac voltage and dc bias voltage, the system response changes from periodic motion to chaotic motion, and then returns to periodic motion.

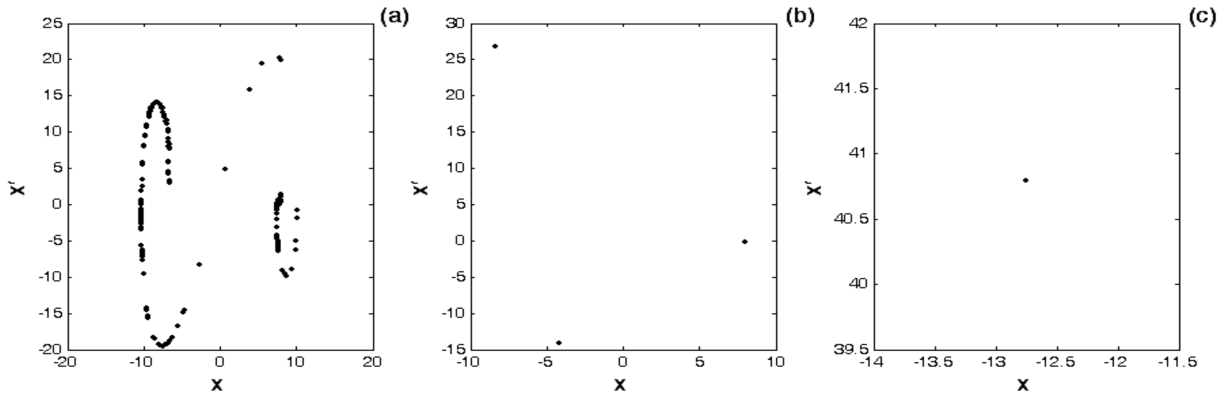

Fig. 10. Poincare maps on the responses of coupling system with different squeeze film damping ratio: (a) $\beta = 0.04$; (b) $\beta = 0.1$; (c) $\beta = 0.2$.

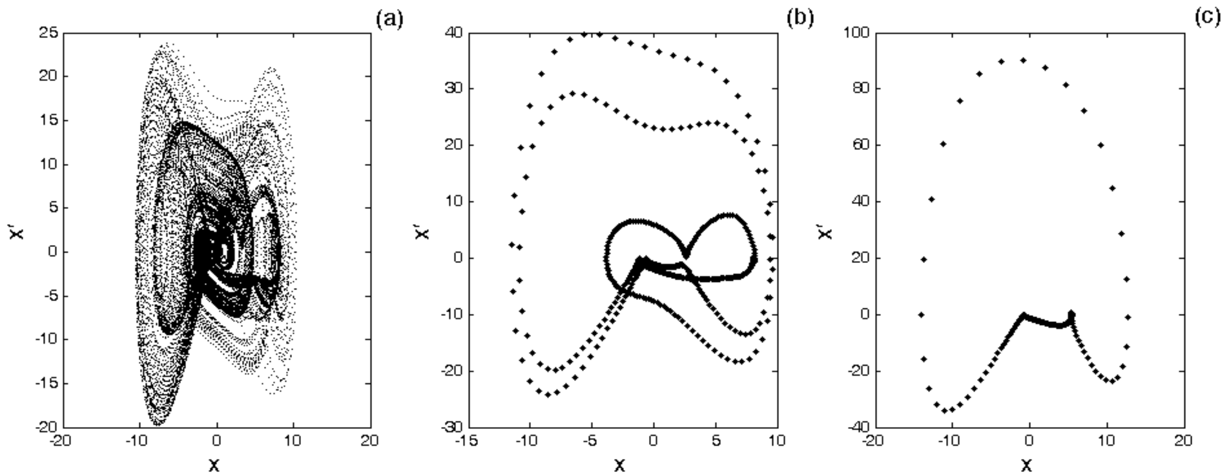

Fig. 11. Phase plane portraits on the responses of coupling system with different squeeze film damping ratio: (a) $\beta = 0.04$; (b) $\beta = 0.1$; (c) $\beta = 0.2$.

5. Conclusions

We have presented analytical and numerical study of the effect of squeeze film damping on the dynamic responses and nonlinear dynamics of the electrostatically actuated MEMS cantilever resonators under combination resonant condition. The effect of nonlinear squeeze film damping on the frequency response, quality factor, resonant frequency and nonlinear dynamic characteristics of the dynamic system are provided using the bifurcation diagram, Poicare maps, largest Lyapunov exponent and phase portrait. The results show the effective stiffness decreases periodically with the increase of the ac voltage and dc bias voltage and the resonant frequency increases with the increase of the gap at the same dc bias voltage. In addition, the resonant frequency is a monotonically decreasing function of increasing dc bias voltage when the ac voltage has not been considered. It is demonstrated that decreasing the squeeze film damping will result in the increase of the quality of the MEMS resonators, which is regarded as a positive phenomenon. The dynamic system responses display very rich nonlinear dynamic characteristics under the effects of squeeze film damping, ac voltage and dc bias voltage, and show an alternate charging process beween the periodic motion and chaotic motion. The mass-spring-damping dynamic model of the electrostatically actuated MEMS resonator utilized in this work could be used to predict the dynamic responses for various parameters qualitatively and in some cases even quantitatively. Characteristic nonlinear dynamic steady-state behaviour is also very well predicted by this simplified dynamic model. It is indicated that both the analytical model and the numerical

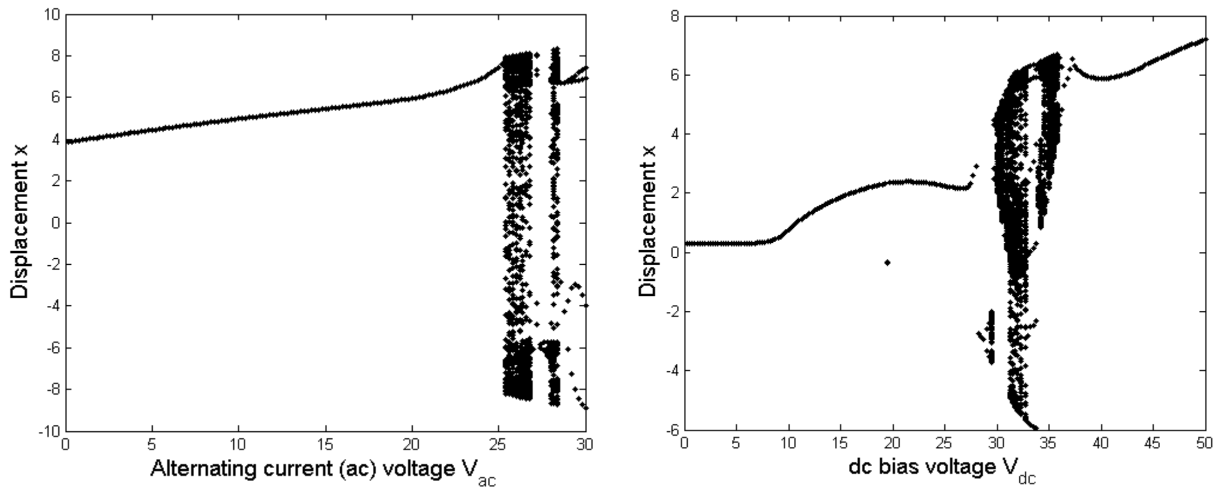

Fig. 12. Bifurcation diagram of (a) ac voltage V_{ac} with $V_{dc} = 40$V, and (b) dc bias voltage V_{dc} with $V_{ac} = 20$V for the coupling nonlinear dynamic system.

simulations can be used very effectively to explain the effect of squeeze film damping on the dynamic responses of the MEMS resonators.

Acknowledgements

This work was supported by the National Science Foundation of China under Grant No. 10602033, the National Outstanding Youth Foundation of China under Grant No.10325209, and the Specialized Research Fund for State Key Laboratory of Mechanical System and Vibration under Grant No. MSV-MS-2008-15.

References

[1] M.S. El Naschie, Nanotechnology for the developing world, *Chaos Solitons & Fractals* **30** (2006), 769–773.
[2] M.I. Younis, F. Alsaleem and D. Jordy, The response of clamped-clamped microbeams under mechanical shock, *International Journal of Non-Linear Mechanics* **42**(4) (2007), 643–657.
[3] M.I. Younis, E.M. Abdel-Rahman and A.H. Nayfeh, Dynamic simulations of a novel RF MEMS switch, *Proc 7th Int Conf on Modeling and Simulation of Microsystems: NanoTech* (*Boston, MA*), 2004, pp. 287–290.
[4] L. Lin, C.T.C. Nguyen, R.T. Howe and A.P. Pisano, Microelectromechanical filters for signal processing, *Proc IEEE Micro Electro Mechanical Systems MEMS '92* (*Travemunde, Germany*), 1992, pp. 226–231.
[5] W. Zhang, R. Baskaran and K.L. Turner, Effect of cubic nonlinearity on auto-parametrically amplified resonant MEMS mass sensor, *Sensors and Actuators A: Physical* **102** (2002), 139–150.
[6] D.W. Carr, S. Evoy, L. Sekaric, H.G. Craighead and J.M. Parpia, Parametric amplification in a torsional microresonator, *Appl Phys Lett* **77** (2000), 1545–1547.
[7] M. Zalalutdinov, A. Olkhovets, B. Ilic, D. Czaplewski and H.G. Craighead, Optically pumped parametric amplification for micromechanical oscillators, *Appl Phys Lett* **78** (2001), 3142-3144.
[8] M.F. Yu and G.J. Wagner, High order parametric resonance and nonlinear mechanics of nanowires, *Technical Proc Nanotechnology Conf and Trade Show* (*San Francisco, CA*) **3** (2003), 325-328.
[9] E.M. Abdel-Rahman and A.H. Nayfeh, Secondary resonances of electrically actuated resonant microsensors, *J Micromech Microeng* **13** (2003), 491–501.
[10] B.J. Gallacher, J.S. Burdess, A.J. Harris and J. Hedley, The application of parametric excitation to a micro-ring gyroscope, *Technical Proc Nanotechnology Conf and Trade Show* (*Boston, MA*) **1** (2004), 359–362.
[11] R. Lifshitz and M.C. Cross, Response of parametrically driven nonlinear coupled oscillators with application to micromechanical and nanomechanical resonator arrays, *Phys Rev B* **67** (2003), 1343021.
[12] B.J. Gallacher, J.S. Burdess and K.M. Harish, A control scheme for a MEMS electrostatic resonant gyroscope excited using combined parametric excitation and harmonic forcing, *J Micromech Microeng* **16** (2006), 320–331.
[13] M. Napoli, R. Baskaran, K.L. Turner and B. Bamieh, Understanding mechanical domain parametric resonance in microcantilevers, *Proc IEEE 16th Int Annual Conf on MEMS*, 2003, pp. 169–172.

[14] E. Buks and M.L. Roukes, Electrically tunable collective response in a coupled micromechanical array, *J Microelectromech Syst* **11** (2002), 802-807.

[15] Y.C. Hu, C.M. Chang and S.C. Huang, Some design considerations on the electrostatically actuated microstructures, *Sensors and Actuators A: Physical* **112** (2004), 155-161.

[16] R. Baskaran and K.L. Turner, Mechanical domain coupled mode parametric resonance and amplification in a torsional mode micro electro mechanical oscillator, *J Micromech Microeng* **13** (2003), 701-707.

[17] K.L. Turner, S.A. Miller, P.G. Hartwell, N.C. MacDonald, S.H. Strogatz and S.G. Adams, Five parametric resonances in a micromechanical system, *Nature* **396** (1998), 149–152.

[18] S. Krylov, I. Harari and Y. Cohen, Stabilization of electrostatically actuated microstructures using parametric excitation, *J Micromech Microeng* **15** (2005), 1188–1204.

[19] M.I. Younis and A.H. Nayfeh, A study of the nonlinear response of a resonant microbeam to electric actuation, *Nonlinear Dynamics* **31** (2003), 91–117.

[20] W.M. Zhang and G. Meng, Nonlinear dynamical system of micro-cantilever under combined parametric and forcing excitations in MEMS, *Sensors and Actuators A: Physical* **119** (2005), 291–299.

[21] A.H. Nayfeh and M.I. Younis, Dynamics of MEMS resonators under superharmonic and subharmonic excitations, *J Micromech Microeng* **15** (2005), 1840–1847.

[22] W.M. Zhang, G. Meng and D. Chen, Stability, nonlinearity and reliability of electrostatically actuated MEMS devices, *Sensors* **7** (2007), 760–796.

[23] R.M.C. Mestrom, R.H.B. Fey, J.T.M. Van Beek, K.L. Phan and H. Nijmeijer, Modelling the dynamics of a MEMS resonator: simulations and experiments, *Sensors and Actuators A: Physical* **142** (2008), 306–315.

[24] N. Kacem, S. Hentz, D. Pinto B. Reig and V. Nguyen, Nonlinear dynamics of nanomechanical beam resonators: improving the performance of NEMS-based sensors, *Nanotechnology* **20** (2009), 275501(11pp).

[25] F.M. Alsaleem, M.I. Younis and H.M. Ouakad, On the nonlinear resonances and dynamic pull-in electrostatically actuated resonators, *J Micromech Microeng* **19** (2009), 045013(14pp).

[26] W.M.Zhang and G. Meng, Nonlinear dynamic analysis of electrostatically actuated resonant MEMS sensors under parametric excitation, *IEEE Sensors Journal* **7**(3) (2007), 370–380.

[27] S.K. De and N.R. Aluru, Complex nonlinear oscillations in electrostatically actuated microstructures, *Journal of Microelectromechanical Systems* **15**(2) (2006), 355–369.

[28] S.K. De and N.R. Aluru, Full-Lagrangian schemes for dynamic analysis of electrostatic MEMS, *Journal of Microelectromechanical Systems* **13**(5) (2004), 737–758.

[29] S. Liu, A. Davidson and Q. Lin, Simulating nonlinear dynamics and chaos in a MEMS cantilever using Poincare mapping, *IEEE the 12th International Conference on Solid State Sensors, Actuators and Microsystems*, Boston, June 8–12, 2003, pp. 1092–1095.

[30] J.E. Sader, Frequency response of cantilever beams immersed in viscous fluids with applications to the atomic force microscope, *J Appl Phys* **84** (1998), 64–76.

[31] S. Basak and A. Raman, Hydrodynamic loading of microcantilevers vibrating in viscous fluids, *J Appl Phys* **99** (2006), 114906.

[32] J.B. Starr, Squeeze-film damping in solid-state accelerometers, *Proc. IEEE Solid State Sensor and Actuator Workshop*, Hilton Head Island, SC, USA, June 4–7, 1990, pp. 44–47.

[33] P.B. Chu, P.R. Nelson, M.L. Tachiki and K.S. Pister, Dynamics of polysilicon parallel-plate electrostatic actuator, *Sensors and Actuators A: Physical* **52** (1996), 216–220.

[34] A.H. Nayfeh, *Perturbation methods*, Wiley, New York, 1973.

Journal of
Engineering

The Scientific
World Journal
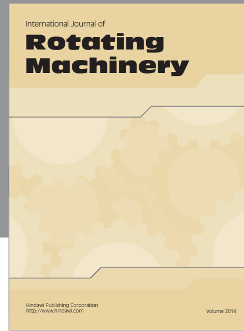
International Journal of
Rotating
Machinery

Journal of
Sensors

International Journal of
Distributed
Sensor Networks
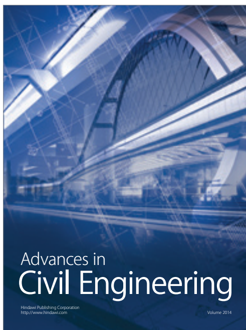
Advances in
Civil Engineering

Hindawi
Submit your manuscripts at
http://www.hindawi.com
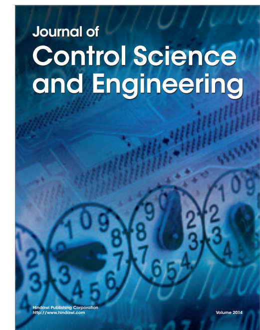
Journal of
Control Science
and Engineering

Journal of
Robotics
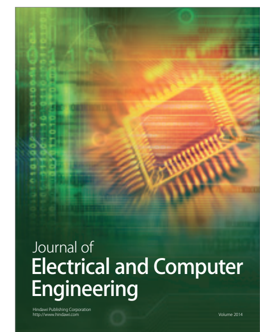
Journal of
Electrical and Computer
Engineering
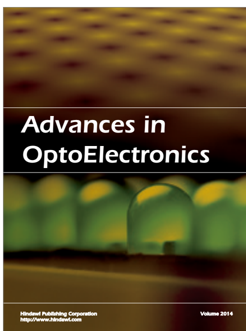
Advances in
OptoElectronics

VLSI Design

International Journal of
Navigation and
Observation
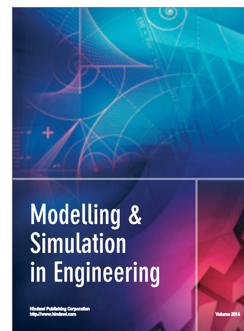
Modelling &
Simulation
in Engineering

International Journal of
Aerospace
Engineering

International Journal of
Chemical Engineering
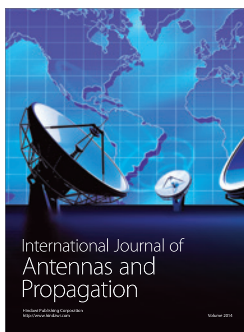
International Journal of
Antennas and
Propagation
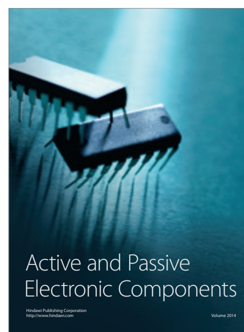
Active and Passive
Electronic Components
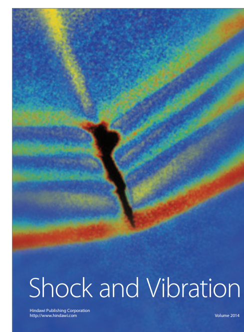
Shock and Vibration
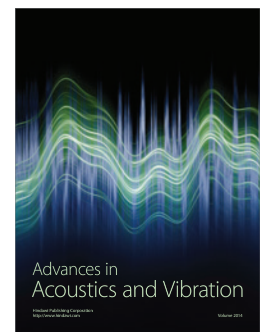
Advances in
Acoustics and Vibration